THE JOURNAL OF PHYSICAL CHEMISTRY A

Article

pubs.acs.org/JPCA

Electronic Structure and Chemical Bonding of a Highly Stable and Aromatic Auro−Aluminum Oxide Cluster

Gary V. Lopez, Tian Jian, Wei-Li Li, and Lai-Sheng Wang*

Department of Chemistry, Brown University, Providence, Rhode Island 02912, United States

Supporting Information

ABSTRACT: We have produced an auro−aluminum oxide cluster, $Au_2(AlO)_2^-$, as a possible model for an Au−alumina interface and investigated its electronic and structural properties using photoelectron spectroscopy and density functional theory. An extremely large energy gap (3.44 eV) is observed between the lowest unoccupied and the highest occupied molecular orbitals of $Au_2(AlO)_2$, suggesting its high electronic stability. The global minima of both $Au_2(AlO)_2^-$ and $Au_2(AlO)_2$ are found to have D_{2h} symmetry with the two Au atoms bonded to the Al atoms of a nearly square-planar $(AlO)_2$ unit. Chemical bonding analyses reveal a strong σ bond between Au and Al, as well as a completely delocalized π bond over the $(AlO)_2$ unit, rendering aromatic character to the $Au_2(AlO)_2$ cluster. The high electronic stability and novel chemical bonding uncovered for $Au_2(AlO)_2$ suggest that it may be susceptible to chemical syntheses as a stable compound if appropriate ligands can be found.

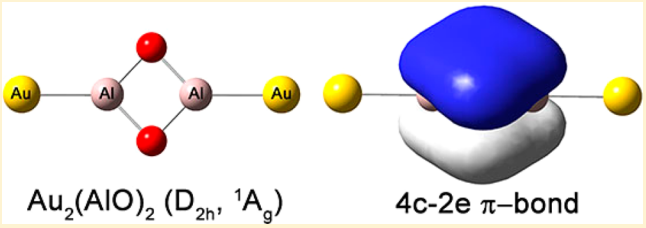

1. INTRODUCTION

Since the discovery of the remarkable catalytic activity of supported gold nanoparticles for low-temperature CO oxidation,[1] intensive studies have been carried out to elucidate the mechanisms of gold catalysts.[2,3] Even though earlier studies have suggested quantum-size effects may play a key role in gold catalysts,[4−9] increasing studies have shown that the cluster−oxide support interface is also critical.[10−15] Size-selected gold clusters have been extensively studied to provide insight into the nature of the catalytic effects of nanogold.[16−24] Recently, tertiary clusters of Au atoms with Ti_xO_y clusters have been produced and their reactivity with CO has been studied as possible models to probe the support effects on the reactivity of gold.[25,26] Alumina is also an important support for gold catalysts.[27−29] Aluminum oxide clusters have been investigated previously as models for oxide catalysts.[30−38] More recent studies have included transition metal-doped aluminum oxides[39−43] and their chemical reactivities.[44,45] But there have been no reports on Au-doped aluminum oxide clusters.

In the current work, we report the observation of a gold aluminum oxide tertiary cluster, $Au_2(AlO)_2^-$, as a possible model for alumina-supported gold. It is characterized by using photoelectron spectroscopy (PES) in an effort to understand the structure and bonding between Au atoms and aluminum oxide. Global minimum searches have led to a D_{2h} structure for both $Au_2(AlO)_2^-$ and its neutral $Au_2(AlO)_2$ with little structural change between the neutral and the anion. Both contain a robust square-planar $(AlO)_2$ unit with the two Au atoms bonded to the Al sites. An extremely large energy gap (3.44 eV) is observed in the PE spectra of $Au_2(AlO)_2^-$, suggesting that neutral $Au_2(AlO)_2$ is an unusually electronically stable molecule. Chemical bonding analyses reveal that the Au atoms form strong covalent bonds with the Al atoms with a calculated bond energy of about 3.3 eV. In addition to the strong Al−O bonds forming the robust $(AlO)_2$ square-planar unit, we also find a completely delocalized π bond. The unusually high stability of $Au_2(AlO)_2$ suggests that it may be viable to be synthesized as a stable compound if appropriate ligands are found for the gold atoms.

2. EXPERIMENTAL AND COMPUTATIONAL METHODS

2.1. Photoelectron Spectroscopy. The experiment was carried out with use of a magnetic-bottle PES apparatus equipped with a laser vaporization supersonic cluster source, details of which can be found elsewhere.[46] Briefly, cluster anions were produced by laser-vaporization of a disk target made of Al and Au (1:4 ratio by mass) in the presence of a helium carrier gas seeded with 5% Ar. The cluster/carrier gas mixture then underwent a supersonic expansion and passed through a skimmer to form a collimated cluster beam into an ion extraction chamber, where a high-voltage pulse extracted the negatively charged clusters into a time-of-flight mass spectrometer. It was observed that residual oxygen contamination on the Al/Au target surface was sufficient to produce various Al/Au oxide clusters. The $Au_2(AlO)_2^-$ cluster was particularly prominent and was selected for the current investigation. It was mass-selected before being photodetached by a laser beam. Four detachment photon energies from either a Nd:YAG laser (532, 355, and 266 nm) or an ArF excimer laser (193 nm) were used in the current work. The variable

Received: April 30, 2014
Revised: June 25, 2014
Published: June 25, 2014

   dx.doi.org/10.1021/jp504236s | J. Phys. Chem. A 2014, 118, 5204−5211

photon energies were important to allow well-resolved spectra to be obtained at low photon energies and to allow high binding energy features to be observed at high photon energies. Photoelectrons were collected at nearly 100% efficiency in a magnetic bottle and analyzed in a 3.5 m long electron flight tube. The PE spectra were calibrated by using the known spectra of Au^-, Pb^-, and Bi^-. The resolution of the apparatus, $\Delta E_k/E_k$, was ~2.5%, i.e., ~25 meV for 1 eV electrons.

2.2. Computational Methods. The search for the global minimum structures of $Au_2(AlO)_2^-$ and $(Al_2O_2)^-$ were performed by using the simulated annealing algorithm,[47−50] coupled with density functional theory (DFT) for geometry optimization. The $(Al_2O_2)^-$ species was studied to compare with the auride species. In the DFT calculations, we used the generalized gradient approximation in the Perdew−Burke−Ernzerhof (PBE) functional form[51] with the Los Alamos ECP plus DZ (LANL2DZ)[52] basis set. The low-lying isomers of $Au_2(AlO)_2^-$ were reoptimized by using PBE0 and the PW91 functionals[53] with the Stuttgart'97[54] and the CRENBL[55] basis sets for gold and the aug-cc-pCVTZ[56,57] basis set for aluminum and oxygen. In the case of the $Al_2O_2^-$ species, the low-lying isomers were reoptimized by using PBE0 and the PW91 functionals with the aug-cc-pCVTZ basis set for aluminum and oxygen. The optimized structures of the anions were used as the starting geometries in the optimization of the neutrals. Harmonic vibrational frequencies were computed to ensure that the low-energy isomers were true minima.

Vertical detachment energies (VDEs) of $Au_2(AlO)_2^-$ were calculated by using the time-dependent DFT (TD-DFT) method.[58] The first VDE was computed as the energy difference between the neutral and the anion at the anion geometry. The excitation energies of deeper orbitals at the anion geometry were then added to the first VDE to give approximate VDEs of the excited states. Each VDE was fitted with a 0.05 eV width Gaussian to yield the simulated PE spectrum. All the calculations were done with NWChem.[59] Additionally, spin−orbit interactions for the gold atom were considered at the PW91 level of theory and the CRENBL basis set with SO potentials,[55] as implemented in NWChem.

To understand the chemical bonding in the closed-shell $Au_2(AlO)_2$, we carried out electron localization analyses using the adaptive natural density partitioning (AdNDP) method[60] on the PW91/LANL2DZ results obtained from Gaussian 09.[61] The AdNDP analysis is based on the concept of electron pairs as the main elements of the chemical bonds. It represents the molecular electronic structure in terms of *n*-center two-electron (*n*c-2e) bonds, recovering the familiar lone pairs (1c-2e) and localized 2c-2e bonds or delocalized *n*c-2e bonds ($3 \le n \le$ total number of atoms in the system). The Gaussview program[62] is used for molecular structure and AdNDP bond visualizations.

Nucleus Independent Chemical Shift (NICS) calculations[63−65] were carried out in Gaussian 09 at the PW91 level of theory, using the LANL2DZ basis set at the PW91/Al,O/Aug-cc-pCVTZ/Au/Stuttgart'97 optimized geometries. NICS values[64,65] were taken as the negative of the isotropic shielding calculated at the center of the $(AlO)_2$ unit in each molecule.

To assess the Au−Al bond strength in $Au_2(AlO)_2$, we calculated the fragmentation energy (ΔE) according to

$$\Delta_1 E[Au_2(AlO)_2] = E[Au(AlO)_2] + E(Au) - E[Au_2(AlO)_2] \quad (1)$$

$$\Delta_2 E[Au(AlO)_2] = E[(AlO)_2] + E(Au) - E[Au(AlO)_2] \quad (2)$$

Similar to the calculations done for the $Au_2(AlO)_2$ species, the energy of the optimized $Au(AlO)_2$ fragment was obtained by using PBE0 and the PW91 functionals with the Stuttgart'97 and the CRENBL basis sets for gold and aug-cc-pCVTZ basis set for aluminum and oxygen.

3. EXPERIMENTAL RESULTS

The PE spectra of $Au_2(AlO)_2^-$ at four different photon energies are displayed in Figure 1. In each spectrum, the X band represents the transition from the anionic ground state to that of the neutral. The A, B, ... bands denote transitions to the excited states of the neutral species. The weak broad PES features labeled with lower case letters (a−d) represent either indirect photodetachment transitions or possible contributions from isomers, as discussed below.

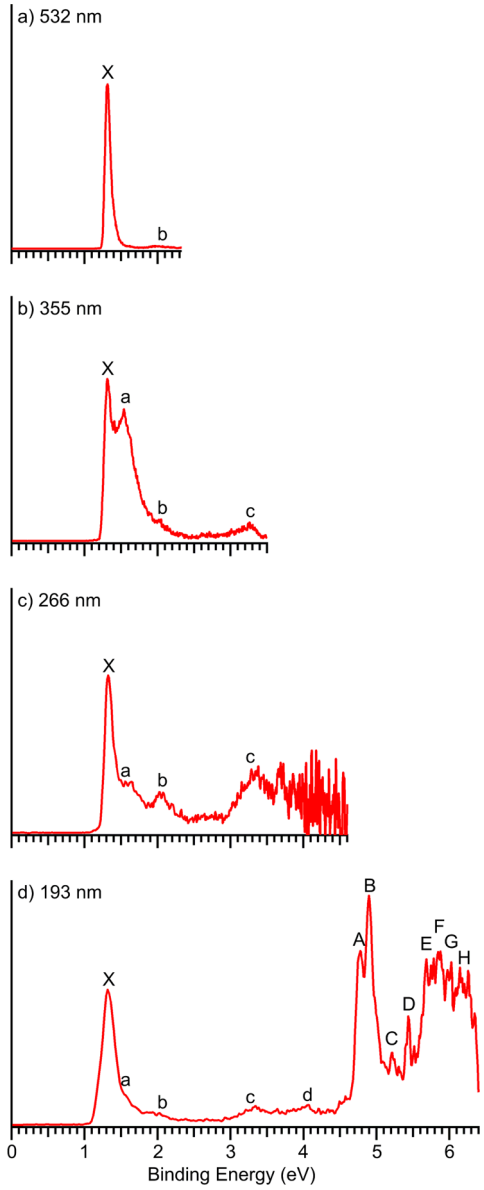

Figure 1. Photoelectron spectra of $Au_2(AlO)_2^-$ at four different photon energies: (a) 532 nm (2.331 eV), (b) 355 nm (3.496 eV), (c) 266 nm (4.661 eV), and (d) 193 nm (6.424 eV).

dx.doi.org/10.1021/jp504236s | J. Phys. Chem. A 2014, 118, 5204−5211

Table 1. Observed Vertical Detachment Energies (VDE) for $Au_2(AlO)_2^-$ in Comparison with the Calculated VDEs for the Global Minimum D_{2h} Structure

obsd features	exptl VDE (eV)[a]	final state and electronic configuration	theoretical VDE (eV)[b]
X	1.34(3)	$^1A_g...b_{3u}^2b_{1g}^2b_{1u}^2b_{2g}^2b_{2u}^2a_u^2a_g^2b_{2g}^2b_{3u}^2a_g^2b_{2u}^2a_g^0$	1.39
A	4.78(5)	$^3B_{2u}...b_{3u}^2b_{1g}^2b_{1u}^2b_{2g}^2b_{2u}^2a_u^2a_g^2b_{2g}^2b_{3u}^2a_g^2b_{2u}^1a_g^1$	4.50
B	4.90(5)	$^3A_g...b_{3u}^2b_{1g}^2b_{1u}^2b_{2g}^2b_{2u}^2a_u^2a_g^2b_{2g}^2b_{3u}^2a_g^1b_{2u}^2a_g^1$	4.69
C	5.21(5)	$^1B_{2u}...b_{3u}^2b_{1g}^2b_{1u}^2b_{2g}^2b_{2u}^2a_u^2a_g^2b_{2g}^2b_{3u}^2a_g^2b_{2u}^1a_g^1$	5.27
D	5.44(5)	$^3B_{3u}...b_{3u}^2b_{1g}^2b_{1u}^2b_{2g}^2b_{2u}^2a_u^2a_g^2b_{2g}^2b_{3u}^1a_g^2b_{2u}^2a_g^1$	5.51
		$^1A_g...b_{3u}^2b_{1g}^2b_{1u}^2b_{2g}^2b_{2u}^2a_u^2a_g^2b_{2g}^2b_{3u}^2a_g^1b_{2u}^2a_g^1$	5.61
E	5.69(7)	$^3B_{2g}...b_{3u}^2b_{1g}^2b_{1u}^2b_{2g}^2b_{2u}^2a_u^2a_g^2b_{2g}^1b_{3u}^2a_g^2b_{2u}^2a_g^1$	5.64
		$^1B_{3u}...b_{3u}^2b_{1g}^2b_{1u}^2b_{2g}^2b_{2u}^2a_u^2a_g^2b_{2g}^2b_{3u}^1a_g^2b_{2u}^2a_g^1$	5.71
F	5.88 (7)	$^1B_{2g}...b_{3u}^2b_{1g}^2b_{1u}^2b_{2g}^2b_{2u}^2a_u^2a_g^2b_{2g}^1b_{3u}^2a_g^2b_{2u}^2a_g^1$	5.77
G	6.03 (7)	$^3A_u...b_{3u}^2b_{1g}^2b_{1u}^2b_{2g}^2b_{2u}^2a_u^1a_g^2b_{2g}^2b_{3u}^2a_g^2b_{2u}^2a_g^1$	6.02
		$^3B_{2u}...b_{3u}^2b_{1g}^2b_{1u}^2b_{2g}^2b_{2u}^1a_u^2a_g^2b_{2g}^2b_{3u}^2a_g^2b_{2u}^2a_g^1$	6.02
		$^3A_g...b_{3u}^2b_{1g}^2b_{1u}^2b_{2g}^2b_{2u}^2a_u^2a_g^1b_{2g}^2b_{3u}^2a_g^2b_{2u}^2a_g^1$	6.02
		$^3B_{2g}...b_{3u}^2b_{1g}^2b_{1u}^2\ b_{2g}^1b_{2u}^2a_u^2\ a_g^2b_{2g}^2b_{3u}^2a_g^2b_{2u}^2a_g^1$	6.02
		$^3B_{3u}...b_{3u}^1b_{1g}^2b_{1u}^2b_{2g}^2b_{2u}^2a_u^2a_g^2b_{2g}^2b_{3u}^2a_g^2b_{2u}^2a_g^1$	6.10
		$^1A_u...b_{3u}^2b_{1g}^2b_{1u}^2b_{2g}^2b_{2u}^2a_u^1a_g^2b_{2g}^2b_{3u}^2a_g^2b_{2u}^2a_g^1$	6.20
H	6.15 (7)	$^1B_{2u}...b_{3u}^2b_{1g}^2b_{1u}^2b_{2g}^2b_{2u}^1a_u^2a_g^2b_{2g}^2b_{3u}^2a_g^2b_{2u}^2a_g^1$	6.21
		$^1B_{2g}...b_{3u}^2b_{1g}^2b_{1u}^2b_{2g}^1b_{2u}^2a_u^2a_g^2b_{2g}^2b_{3u}^2a_g^2b_{2u}^2a_g^1$	6.21
		$^1A_g...b_{3u}^2b_{1g}^2b_{1u}^2b_{2g}^2b_{2u}^2a_u^2a_g^1b_{2g}^2b_{3u}^2a_g^2b_{2u}^2a_g^1$	6.21
		$^3B_{1u}...b_{3u}^2b_{1g}^2b_{1u}^1b_{2g}^2b_{2u}^2a_u^2a_g^2b_{2g}^2b_{3u}^2a_g^2b_{2u}^2a_g^1$	6.37

[a]Numbers in parentheses present experimental uncertainties in the last digit. [b]Calculated at the PW91/Al,O/Aug-cc-pCVTZ/Au/Stuttgart'97 level of theory.

The 532-nm spectrum (Figure 1a) displays one sharp feature X with a VDE of 1.34 ± 0.03 eV. Because no vibrational structures were resolved, the adiabatic detachment energy (ADE) of this band was estimated by drawing a straight line along the rising edge band X and then adding the instrumental resolution to its intersection with the binding energy axis. The ADE so determined is 1.27 ± 0.03 eV, which also represents the electron affinity (EA) of neutral $Au_2(AlO)_2$. The sharp onset and narrow width of feature X suggest little geometry change between the anion ground state and that of the neutral. The PE spectrum at 193 nm (Figure 1d) shows a very large energy gap between bands X and A, filled with broad and weak signals (a–d). Band A at a VDE of 4.78 ± 0.05 eV is quite sharp and intense, followed by an even more intense and sharp peak B at a VDE of 4.90 ± 0.05 eV. Two sharp and weaker peaks C and D are observed at VDEs of 5.21 and 5.44 eV, respectively. Beyond peak D, the 193 nm spectrum becomes very congested and it is difficult to identify individual detachment bands. A number of peaks (E to H) are labeled for the sake of discussion. The VDEs of all the major detachment bands are given in Table 1, where they are compared with the theoretical results.

The large separation of 3.44 eV between bands X and A suggests that neutral $Au_2(AlO)_2$ is closed shell and the X–A gap can be viewed approximately as the energy gap between its lowest unoccupied (LUMO) and highest occupied (HOMO) molecular orbitals. The 3.44 eV HOMO–LUMO gap, which is also borne out of the theoretical calculations, is extremely large. Surprisingly, numerous weak and broad features (a–d) are observed in the X and A band gap region. Features a (1.57 eV) and b (~2.1 eV) exhibit strong photon-energy dependence, in particular, feature a, which does not exist at 532 nm (Figure 1a) and becomes very strong at 355 nm (Figure 1b). Feature b also displays dependence on the photon energy, being the strongest at 266 nm (Figure 1c). These photon-energy dependences bear the signature of autodetachment, in which an anion excited state is produced upon resonant absorption of a detachment photon. Strong autodetachment has been observed previously in anion PES for clusters with very large HOMO–LUMO gaps, such as C_{60}, Cr_2, and Au_{20}.[66−68] Features *c* (~3.4 eV) and *d* (~4.1 eV) do not show too strong photon energy dependence, and they are likely due to contributions from a low-lying isomer (vide infra).

4. THEORETICAL RESULTS AND COMPARISON WITH EXPERIMENT

4.1. The Optimized Structures of $Au_2(AlO)_2^-$ and $Au_2(AlO)_2$. The simple Al_2O_2 cluster has been calculated previously by various levels of theory and found to be a closed-shell species (^1A_g) with D_{2h} symmetry.[30,69,70] High-level CCSD(T) calculations predicted an Al–O bond length of 1.766 Å and a ∠O–Al–O bond angle of 93.6°.[70] The reliability of the present computational methods was validated by performing calculations on the anion and neutral species of Al_2O_2. As shown in Figure 2a,b, our PW91 results for the Al–O bond lengths, 1.769 and 1.745 Å, and the ∠O–Al–O bond angle, 91.9° and 93.1°, for $Al_2O_2^-$ and Al_2O_2, respectively, are in good agreement with the previous results.

The global minimum of $Au_2(AlO)_2^-$ was searched extensively at the PBE0 and PW91 levels of theory. Only four structures were found within 50 kcal/mol of the global minimum, as shown in Figure S1 in the Supporting Information. The most stable structure of $Au_2(AlO)_2^-$ (Figure 2c) is found to be D_{2h} with a nearly square-planar $(AlO)_2$ unit, where the two Au atoms are bonded to the two Al atoms, respectively. Since both PBE0 and PW91 give similar results (Figure S1, Supporting Information), we will use the PW91 results in our discussion. The nearest low-lying isomer is 11 kcal/mol higher in energy, in which a gold dimer is bonded to a $(AlO)_2$ unit on one side with an Au–Au bond (isomer I in Figure S1, Supporting Information). Both isomers II and III are more than 30 kcal/mol higher in energy (Figure S1, Supporting

dx.doi.org/10.1021/jp504236s | J. Phys. Chem. A 2014, 118, 5204–5211

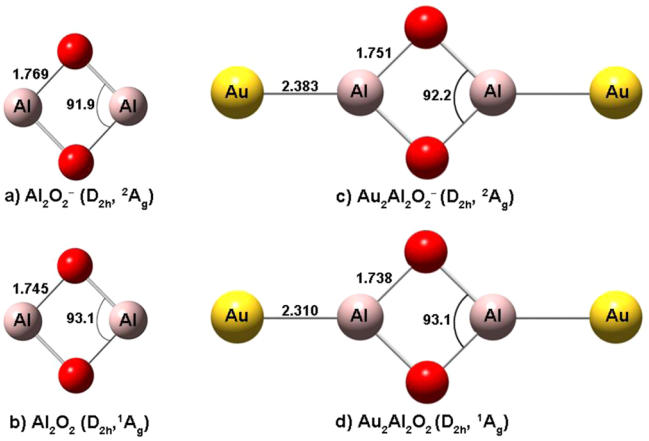

Figure 2. Optimized structures for $Al_2O_2^-$ (a) and Al_2O_2 (b) and their point group symmetries and electronic states at the PW91/Al,O/Aug-cc-pCVTZ level of theory and the optimized structures for $Au_2(AlO)_2^-$ (c) and $Au_2(AlO)_2$ (d) and their point group symmetries and electronic states at the PW91/Al,O/Aug-cc-pCVTZ/Au/Stuttgart'97 level of theory. Bond lengths are given in Å and bond angles in degrees.

Information). We optimized the structure of neutral $Au_2(AlO)_2$ based on the global minimum of the anion and found it to have an almost identical structure as $Au_2(AlO)_2^-$ except the Au−Al bond length is slightly reduced by 0.073 Å upon electron detachment (Figure 2d). The $(AlO)_2$ unit seems to be extremely robust and has similar Al−O bond lengths and ∠O−Al−O bond angles, in both $Au_2(AlO)_2^-$ and $Au_2(AlO)_2$, as well as in $Al_2O_2^-$ and Al_2O_2 (Figure 2). In both cases, $Au_2(AlO)_2^-$ and $Au_2(AlO)_2$, the structures are found to be planar where the ∠Au−Al−Al angle is 180°.

4.2. Comparison between the Experimental and Theoretical Results. To confirm the global minimum structure, we calculated the ADE and VDEs of the optimized structures for comparison with the experiment. The calculated ADE and the first VDE at different levels of theory and basis sets are compared in Table 2 for the global minimum D_{2h} structure. It was found that no significant improvement was observed when including spin−orbit interactions in our calculations. Since our calculations at PW91/Al,O/Aug-cc-pCVTZ/Au/Stuttgart'97 give the ADE and the first VDE in good agreement with the experimental data, this level of theory and basis set were used to simulate the PE spectrum.

Table 2. Calculated Adiabatic Detachment Energy (ADE) and First Vertical Detachment Energy (VDE) at Different Levels of Theory and Basis Sets (for Au) for the D_{2h} Global Minimum of $Au_2(AlO)_2^-$ in Comparison with the Experimental Values[a]

		ADE	first VDE
PBE0	Au/Stuttgart'97	1.33	1.38
	Au/CRENBL	1.40	1.45
PW91	Au/Stuttgart'97	1.34	1.39
	Au/CRENBL	1.41	1.46
	Au/CRENBL-SO[b]	1.44	1.49
experiment		1.27 ± 0.03	1.34 ± 0.03

[a]The Al,O/Aug-cc-pCVTZ basis set was used in all cases. All energies are in eV. [b]SO: spin−orbit effects included.

All the calculated VDEs from the global minimum of $Au_2(AlO)_2^-$ at the PW91 level are compared with the experimental data in Table 1. The valence molecular orbitals (MOs) for $Au_2(AlO)_2$ are displayed in Figure 3; the LUMO (a_g, Figure S3, Supporting Information) where the extra electron resides in the anion is a nonbonding MO mainly of Au 6s character with slight antibonding interaction with Al. The calculated first VDE from removal of the electron in the SOMO (a_g) of the anion is 1.39 eV, in excellent agreement with the experimental value of 1.34 eV. The nature of the SOMO [corresponding to the LUMO of $Au_2(AlO)_2$] is consistent with the slight reduction of the Au−Al bond length upon electron detachment and the relatively sharp ground state PES band. We computed the vibrational frequency of the totally symmetric mode involving Au−Al stretching to be 109 cm^{-1}, which is beyond the resolution of our magnetic bottle PES analyzer. The ground state X band in the PE spectra should contain a short vibrational progression in the Au−Al stretching mode. The second detachment channel occurs from the HOMO (b_{2u}), leaving the final neutral species in the lowest triplet state ($^3B_{2u}$). The calculated VDE of this detachment channel is 4.50 eV, in good accord with band A at 4.78 eV. The computed X−A separation of 3.11 eV is very large, in good agreement with the observed value of 3.44 eV. The corresponding detachment from the HOMO into the singlet final state ($^1B_{2u}$) gives a calculated VDE of 5.27 eV, in good agreement with band C at 5.21 eV. The relative intensities of bands A and C are consistent with the spin multiplicities of the final states.

The third detachment channel from HOMO−1 (a_g) to the triplet final state (^3A_g) is calculated to be at 4.69 eV, consistent with band B at 4.90 eV. The corresponding detachment to the singlet final state (^1A_g) is calculated to be at 5.61 eV, in good agreement with band E at 5.69 eV. The next detachment is from HOMO−2 (b_{3u}) with a calculated VDE of 5.51 eV, agreeing well with band D at 5.44 eV. Beyond 5.5 eV, the experimental PE spectrum becomes highly congested. This observation is in excellent agreement with the calculated VDEs for the higher binding energy detachment channels, which are mostly from the Au 5d manifold, as shown in Table 1 and Figure 3. Overall, the calculated VDEs for the D_{2h} structure for $Au_2(AlO)_2^-$ are in excellent agreement with the experimental data, unequivocally confirming it as the global minimum.

The simulated PE spectrum of the global minimum, as well as those from isomers I to III, is compared with the 193 nm spectrum in Figure S2 (Supporting Information). The excellent agreement between that of the global minimum and the experiment is obvious. Isomers II and III can be safely ruled out because they are significantly higher in energy. Their simulated spectra show no resemblance to the weak features observed. However, the first two bands of the simulated spectrum from isomer I are in the same energy range as the weak features c and d, which are tentatively attributed to contributions from isomer I. The higher binding energy detachment features from isomer I would be buried in the congested features of the global minimum.

5. DISCUSSION

The 3.44 eV HOMO−LUMO gap observed for $Au_2(AlO)_2$ sets a record, the largest of any clusters that we have ever observed. This very large energy gap is greater than that observed in highly stable and chemically inert systems like C_{60} (1.57 eV)[68] or even Au_{20} (1.77 eV).[68] The unprecedentedly large HOMO−LUMO gap implies that neutral $Au_2(AlO)_2$ is an extremely

dx.doi.org/10.1021/jp504236s | J. Phys. Chem. A 2014, 118, 5204−5211

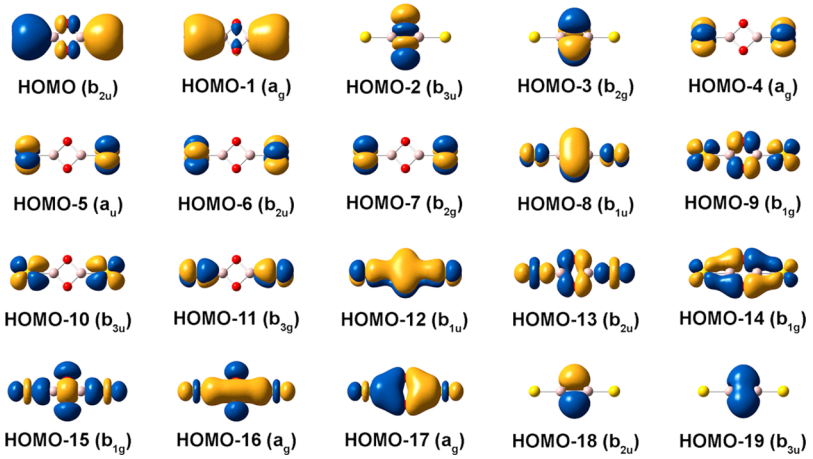

Figure 3. Occupied valence molecular orbitals of the D_{2h} $Au_2(AlO)_2$ at PW91/Al,O/Aug-cc-pCVTZ/Au/Stuttgart'97 level of theory.

stable electronic system. We performed AdNDP analyses to gain insight into its stability and chemical bonding, as presented in Figure 4. We found 12 lone pairs, which belong to the 5d

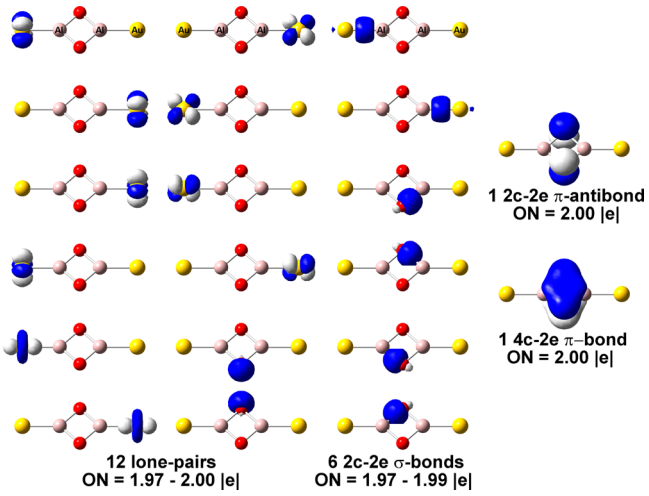

Figure 4. Results of AdNDP analyses for $Au_2(AlO)_2$. ON denotes the occupation number.

orbitals for the two Au atoms and two O 2s orbitals all with occupation numbers very close to 2 |e|. The Au−Al and Al−O bonds are each represented by a classical 2c−2e σ bond with occupation numbers also very close to 2 |e|. We found a 4c−2e π bond completely delocalized on $(AlO)_2$ square-planar unit, as well as an antibonding π bond, which are localized on the two O atoms. These two bonds are basically the bonding and antibonding combinations of the O $2p_z^2$ electrons (HOMO−3 and HOMO−8 in Figure 3). However, the bonding combination involves electron delocalization into the empty Al $3p_z$ orbitals. Hence, the bonding π bond is not canceled by the localized antibonding orbital and the 4c−2e bond should render aromaticity for the $(AlO)_2$ square-planar unit.

To evaluate the aromaticity of the $(AlO)_2$ unit in $Au_2(AlO)_2$, we computed the NICS values within and above the molecular plane at the PW91 level of theory. The NICS values at the geometrical center of the molecule [NICS(0)] contain important contributions from the in-plane tensor components that are not related to aromaticity.[71,72] NICS(1) corresponding to 1 Å above or below the plane of the molecule reflects essentially the π effects and it is a better indicator of the ring current than the value at the center since at 1 Å the effects of the local σ-bonding contributions are diminished.[71,72] Significant negative NICS values imply aromaticity, while positive values correspond to antiaromaticity. Nonaromatic cyclic systems should have NICS values around zero. In Table 3,

Table 3. Comparison of the NICS Values Calculated for the D_{2h} $Au_2(AlO)_2$ with Those of Benzene and Cyclobutadiene (C_4H_4)

	$Au_2(AlO)_2$	C_4H_4	benzene
NICS(0)	−12.2	26.1	−7.8
NICS(1)	−5.9	16.7	−10.0

we compare the NICS values of $Au_2(AlO)_2$ with those of benzene, a prototypical aromatic molecule, and those of cyclobutadiene (C_4H_4), a prototypical antiaromatic molecule. The results suggest that $Au_2(AlO)_2$ is indeed highly aromatic, consistent with the robustness of the $(AlO)_2$ unit and its nearly square-planar structure.

Because of the difference between the electronegativities of Al and O, there is no doubt that the Al−O bonds contain strong ionic characters. From the covalent point of view, the nearly 90° bond angles in the $(AlO)_2$ square-planar unit mean that both Al and O can simply use their valence p_x and p_y orbitals to form bonds with each other without the need of hybridization. Indeed, the two lone pairs on the O atoms are mainly O 2s, corresponding to the two deepest MOs (HOMO−18 and HOMO−19 in Figure 3). However, for Al a 3s electron needs to be promoted to the 3p level so it can have the $3p_x^1p_y^1$ configuration to bond with the O atoms. A single electron in the 3s orbital of Al can then favorably bond to the Au atoms, forming two strong Al−Au bonds.

To assess the Al−Au bond strength, we calculated the fragmentation energy Δ_1E and Δ_2E, according to eqs 1 and 2. We found that Δ_1E is 3.2 eV and Δ_2E is 3.4 eV, giving an average Al−Au bond strength of 3.3 eV in $Au_2(AlO)_2$. This bond energy is extremely large, compared to either the Al−Al bond strength (1.42 eV)[73] or Au−Au bond strength (2.04 eV),[74] and agrees with the dissociation energy of the AuAl bond measured experimentally to be 3.34 ± 0.07 eV.[75] Hence, the $Au_2(AlO)_2$ cluster represents a very special and stable molecule with an aromatic $(AlO)_2$ square-planar unit and two unusually strong Al−Au bonds. Its special stability is reflected in its

dx.doi.org/10.1021/jp504236s | J. Phys. Chem. A 2014, 118, 5204−5211

unprecedentedly large HOMO−LUMO gap. It is conceivable that it may be synthesized if a bulky neutral ligand can be found to coordinate the Au atoms and protect the $(AlO)_2$ unit. Hence, $Au_2(AlO)_2$ represents a novel molecular species and it may serve as a simple model for Au atoms interacting with O-deficient defect sites on alumina surfaces.

6. CONCLUSIONS

We report the observation and characterization of an auro−aluminum oxide cluster, $Au_2(AlO)_2^-$, and its neutral. Photoelectron spectroscopy revealed a very large energy gap between the first and second detachment bands of $Au_2(AlO)_2^-$ and a relatively low electron affinity of 1.27(3) eV for $Au_2(AlO)_2$. Global minimum searches led to a D_{2h} structure for both the anion and its neutral, in which the two gold atoms are bonded to the two Al atoms, respectively, in a square-planar $(AlO)_2$ unit. The large energy gap (3.44 eV) observed experimentally, which was confirmed theoretically, represents an unprecedentedly large HOMO−LUMO gap for the corresponding neutral $Au_2(AlO)_2$, and suggests that it is an extremely stable electronic system. AdNDP analyses showed that the Al−O and Al−Au bonds are all classical 2c−2e bonds, whereas there is a delocalized π bond over the $(AlO)_2$ square-planar unit, rendering aromaticity to the $Au_2(AlO)_2$ cluster. The nearly square geometry of the $(AlO)_2$ unit suggests that both Al and O do not need hybridization to form chemical bonds in $Au_2(AlO)_2$. Hence the Al atom is left with a 3s electron to form a strong bond with Au, and an empty $3p_z$ orbital, which participates in the delocalized π bond. The Al−Au bond is found to be quite strong with an average calculated bond energy of 3.3 eV. The interesting chemical bonding and high stability of $Au_2(AlO)_2$ suggest that it may be a target for chemical syntheses with suitable ligation to the Au atoms.

■ ASSOCIATED CONTENT

Supporting Information

Low-lying structures of $Au_2(AlO)_2^-$, their energies, computed first vertical detachment energies, and comparison of their simulated photoelectron spectra with experiment. This material is available free of charge via the Internet at http://pubs.acs.org.

■ AUTHOR INFORMATION

Corresponding Author

*E-mail: lai-sheng_wang@brown.edu. Tel: (401) 863-3389.

Notes

The authors declare no competing financial interest.

■ ACKNOWLEDGMENTS

This work was supported by the National Science Foundation (CHE-1049717). The calculations were done with use of resources at the Center for Computation and Visualization (CCV) of Brown University.

■ REFERENCES

(1) Haruta, M. Size- and Support-Dependency in the Catalysis of Gold. *Catal. Today* **1997**, *36*, 153−166.
(2) Cho, A. Connecting the Dots to Custom Catalysts. *Science* **2003**, *299*, 1684−1685.
(3) Hutchings, G. J.; Haruta, M. A. Golden Age of Catalysis: A Perspective. *Appl. Catal., A* **2005**, *291*, 2−5.
(4) Valden, M.; Lai, X.; Goodman, D. W. Onset of Catalytic Activity of Gold Clusters on Titania with the Appearance of Nonmetallic Properties. *Science* **1998**, *281*, 1647−1650.
(5) Sanchez, A.; Abbet, S.; Heiz, U.; Schneider, W. D.; Hakkinen, H.; Barnett, R. N.; Landman, U. When Gold Is Not Noble: Nanoscale Gold Catalysts. *J. Phys. Chem. A* **1999**, *103*, 9573−9578.
(6) Lee, S.; Fan, C.; Wu, T.; Anderson, S. L. CO Oxidation on Aun/TiO_2 Catalysts Produced by Size-Selected Cluster Deposition. *J. Am. Chem. Soc.* **2004**, *126*, 5682−5683.
(7) Lemire, C.; Meyer, R.; Shaikhutdinov, S.; Freund, H. J. Do Quantum Size Effect Control CO Adsorption on Gold Nanoparticles? *Angew. Chem., Int. Ed.* **2004**, *43*, 118−121.
(8) Landman, U.; Yoon, B.; Zhang, C.; Heiz, U.; Arenz, M. Factors in Gold Catalysis: Oxidation of CO in the Non-Scalable Size Regime. *Top. Catal.* **2007**, *44*, 145−158.
(9) Lopez-Acevedo, O.; Kacprzak, K. A.; Akola, J.; Hakkinen, H. Quantum Size Effects in Ambient CO Oxidation Catalyzed by Ligand-Protected Gold Clusters. *Nat. Chem.* **2010**, *2*, 329−334.
(10) Molina, L. M.; Hammer, B. Some Recent Theoretical Advances in the Understanding of the Catalytic Activity of Au. *Appl. Catal., A* **2005**, *291*, 21−31.
(11) Yan, W.; Brown, S.; Pan, Z.; Mahurin, S. M.; Overbury, S. H.; Dai, S. Ultrastable Gold Nanocatalyst Supported by Nanosized Non-Oxide Substrate. *Angew. Chem., Int. Ed.* **2006**, *45*, 3614−3618.
(12) Rodriguez, J. A.; Ma, S.; Liu, P.; Hrbek, J.; Evans, J.; Perez, M. Activity of CeO_x and TiO_x Nanoparticles Grown on Au(111) in the Water-Gas Shift Reaction. *Science* **2007**, *318*, 1757−1760.
(13) Janssens, T. V. W.; Clausen, B. S.; Hvolbak, B.; Falsig, H.; Christensen, C. H.; Bligaard, T.; Norskov, J. K. Insights into the Reactivity of Supported Au Nanoparticles: Combining Theory and Experiments. *Top. Catal.* **2007**, *44*, 15−26.
(14) Herzing, A. A.; Kiely, C. J.; Carley, A. F.; Landon, P.; Hutchings, G. J. Identification of Active Gold Nanoclusters on Iron Oxide Supportsfor CO Oxidation. *Science* **2008**, *321*, 1331−1335.
(15) Green, I. X.; Tang, W.; Neurock, M.; Yates, J. T. Spectroscopic Observation of Dual Catalytic Sites During Oxidation of CO on a Au/TiO_2 Catalyst. *Science* **2011**, *333*, 736−739.
(16) Salisbury, B. E.; Wallace, W. T.; Whetten, R. L. Low-Temperature Activation of Molecular Oxygen by Gold Clusters: A Stoichiometric Process Correlated to Electron Affinity. *Chem. Phys.* **2000**, *262*, 131−141.
(17) Hagen, J.; Socaciu, L. D.; Elijazyfer, M.; Heiz, U.; Bernhardt, T. M.; Woste, L. Coadsorption of CO and O_2 on Small Free Gold Cluster Anions at Cryogenic Temperatures: Model Complexes for Catalytic CO Oxidation. *Phys. Chem. Chem. Phys.* **2002**, *4*, 1707−1709.
(18) Stolcic, D.; Fischer, M.; Gantefor, G.; Kim, Y. D.; Sun, Q.; Jena, P. Direct Observation of Key Reaction Intermediates on Gold Clusters. *J. Am. Chem. Soc.* **2003**, *125*, 2848−2849.
(19) Kimble, M. L.; Castleman, A. W.; Mitric, R.; Burgel, C.; Bonacic-Koutecky, V. Reactivity of Atomic Gold Anions Toward Oxygen and the Oxidation of CO: Experiment and Theory. *J. Am. Chem. Soc.* **2004**, *126*, 2526−2535.
(20) Zhai, H. J.; Kiran, B.; Dai, B.; Li, J.; Wang, L. S. Unique CO Chemisorption Properties of Gold Hexamer: $Au_6(CO)_n^-$ (n = 0−3). *J. Am. Chem. Soc.* **2005**, *127*, 12098−12106.
(21) Nuemaier, M.; Weigend, F.; Hampe, O.; Kappes, M. M. Binding Energy and Preferred Adsorptiion Sites of CO on Gold and Silver-Gold Cluster Cations: Adsorption Kinetics and Quantum Chemical Calculations. *Faraday Discuss.* **2008**, *138*, 393−406.
(22) Haeck, J. D.; Veldeman, N.; Claes, P.; Janssens, E.; Andersson, M.; Lievens, P. Carbon Monoxide Adsorption on Silver Doped Gold Clusters. *J. Phys. Chem. A* **2011**, *115*, 2103−2109.
(23) Woodham, A.; Meijer, G.; Fielicke, A. Activation of Molecular Oxygen by Anionic Gold Clusters. *Angew. Chem., Int. Ed.* **2012**, *51*, 4444−4447.
(24) Pal, R.; Wang, L. M.; Pei, Y.; Wang, L. S.; Zeng, X. C. Unraveling the Mechanisms of O_2 Activation by Size-Selected Gold Clusters: Transition from Superoxo to Peroxo Chemisorption. *J. Am. Chem. Soc.* **2012**, *134*, 9438−9445.
(25) Himeno, H.; Miyajima; Yasuike, T.; Mafune, F. Gas Phase Synthesis of Au Clusters Deposited on Titanium Oxide Clusters and

Their Reactivity with CO Molecules. *J. Phys. Chem. A* **2011**, *115*, 11479−11485.
(26) Li, X. N.; Yuan, Z.; He, S. G. CO Oxidation Promoted by Gold Atoms Supported on Titanium Oxide Cluster Anions. *J. Am. Chem. Soc.* **2014**, *136*, 3617−3623.
(27) Carrey, J.; Maurice, J. L.; Petroff, F.; Vaures, A. Growth of Au Clusters on Amorphous Al_2O_3: Evidence of Cluster Mobility above a Critical Size. *Phys. Rev. Lett.* **2001**, *86*, 4600−4603.
(28) Costello, C. K.; Kung, M. C.; Oh, H. S.; Wang, Y.; Kung, H. H. Nature of the Active Site for CO Oxidation on Highly Active Au/ρ-Al_2O_3. *Appl. Catal., A* **2002**, *232*, 159−168.
(29) Lee, S.; Fan, C.; Wu, T.; Anderson, S. L. Agglomeration, Sputtering, and Carbon Monoxide Adsorption Behavior for Au/Al_2O_3 Prepared by Au_n^+ Depostion on Al_2O_3/NiAl(110). *J. Phys. Chem. B* **2005**, *109*, 11340−11347.
(30) Desai, S. R.; Wu, H.; Rohlfing, C. M.; Wang, L. S. A Sudy of the Structure and Bonding of Small Aluminum Oxide Clusters by Photoelectron Spectroscopy: $Al_xO_y^-$ (x = 1−2, y = 1−5). *J. Chem. Phys.* **1997**, *106*, 1309−1317.
(31) Wu, H.; Li, X.; Wang, X. B.; Ding, C. F.; Wang, L. S. Al_3O_x (x = 0−5) Clusters: Sequential Oxidation, Metal-to-Oxide Transformation, and Photoisomerization. *J. Chem. Phys.* **1998**, *109*, 449−458.
(32) Meloni, G.; Ferguson, M. J.; Neumark, D. M. Negative Ion Photodetachment Spectroscopy of the Al_3O_2, Al_3O_3, Al_4O_x, Al_5O_x (x = 3−5), Al_6O_5, and Al_7O_5 Clusters. *Phys. Chem. Chem. Phys.* **2003**, *5*, 4073−4079.
(33) Das, U.; Raghavachari, K.; Jarrold, C. C. Addition of Water to $Al_5O_4^-$ Determined by Anion Photoelectron Spectroscopy and Quantum Chemical Calculations. *J. Chem. Phys.* **2005**, *122*, 014313.
(34) Guevara-Garcia, A.; Martinez, A.; Ortiz, J. V. Addition of Water, Methanol, and Ammonia to $Al_3O_3^-$ Clusters: Reaction Products, Transition States, and Electron Detachment Energies. *J. Chem. Phys.* **2005**, *122*, 214309.
(35) Santambrogio, G.; Janssens, E.; Li, S.; Siebert, T.; Meijer, G.; Asmis, K. R.; Doebler, J.; Sierka, M.; Sauer, J. Identification of Conical Structures in Small Aluminum Oxide Clusters: Infrared Spectroscopy of $(Al_2O_3)_{1-4}(AlO)^+$. *J. Am. Chem. Soc.* **2008**, *130*, 15143−15149.
(36) Sierka, M.; Döbler, J.; Sauer, J.; Zhai, H. J.; Wang, L. S. The $[(Al_2O_3)_2]^-$ Anion Cluster: Electron Localization-Delocalization Isomerism. *ChemPhysChem* **2009**, *10*, 2410−2413.
(37) Wang, Z. C.; Weiske, T.; Kretscher, R.; Maria, S.; Kaupp, M.; Schwarz, H. Structure of the Oxygen-Rich Cluster Cation $Al_2O_7^+$ and Its Reactivity. *J. Am. Chem. Soc.* **2011**, *133*, 16930−16937.
(38) Tian, L. H.; Ma, T. M.; Li, X. N.; He, S. G. C-H Bond Activation by Aluminum Oxide Cluster Anions, An Experimental and Theoretical Study. *Dalton Trans.* **2013**, *42*, 11205.
(39) Zhang, Z. G.; Xu, H. G.; Zhao, Y. C.; Zheng, W. J. Photoelectron Spectroscopy and Density Functional Theory Study of $TiAlO_y^-$ (y = 1−3) and $TiAl_2O_y^-$ (y = 2−3) Clusters. *J. Chem. Phys.* **2010**, *133*, 154314.
(40) Zhang, Z. G.; Xu, H. G.; Kong, X. Y.; Zheng, W. J. Anion Photoelectron Spectroscopy and Density Functional Study of Small Aluminum-Vanadium Oxide Clusters. *J. Phys. Chem. A* **2011**, *115*, 13−18.
(41) Mann, J. E.; Waller, S. E.; Jarrold, C. C. Electronic Structures of $WAlO_y$ and $WAlO_y^-$ (y = 2−4) Determined by Anion Photoelectron Spectroscopy and Density Functional Theory Calculations. *J. Chem. Phys.* **2012**, *137*, 044301.
(42) Waller, S. E.; Mann, J. E.; Hossain, E.; Troyer, M.; Jarrold, C. C. Electronic Structures of $AlMoO_y^-$ (y = 1−4) Determined by Photoelectron Spectroscopy and Density Functional Theory Calculations. *J. Chem. Phys.* **2012**, *137*, 024302.
(43) Mann, J. E.; Waller, S. E.; Jarrold, C. C. Shift from Covalent to Ionic Bonding in Al_2MoO_y (y = 2−4) Anion and Neutral Clusters. *J. Phys. Chem. A* **2013**, *117*, 12116−12124.
(44) Wang, Z. C.; Wu, X. N.; Zhao, Y. X.; Ma, J. B.; Ding, X. L.; He, S. G. Room-Temperature Methane Activation by a Bimetallic Oxide Cluster $AlVO_4^+$. *Chem. Phys. Lett.* **2010**, *489*, 25.
(45) Wang, Z. C.; Wu, X. N.; Zhao, Y. Z.; Ma, J. B.; Ding, X. L.; He, S. G. C-H Activation on Aluminum-Vanadium Bimetallic Oxide Cluster Anions. *Chem.—Eur. J.* **2011**, *17*, 3449.
(46) Wang, L. S.; Cheng, H. S.; Fan, J. Photoelectron Spectroscopy of Size-Selected Transition Metal Clusters: Fe_n^-, n = 3−24. *J. Chem. Phys.* **1995**, *102*, 9480−9493.
(47) Clark, J.; Call, S. T.; Austin, D. E.; Hansen, J. C. Computational Study of Isoprene Hydroxyalkyl Peroxy Radical Water Complexes $(C_5H_8(OH)O_2\text{-}H_2O$. *J. Phys. Chem. A* **2010**, *114*, 6534−6541.
(48) Averkiev, B. B.; Call, S.; Boldyrev, A. I.; Wang, L. M.; Huang, W.; Wang, L. S. Photoelectron Spectroscopy and Ab initio Study of the Structure and Bonding of Al_7N^- and Al_7N. *J. Phys. Chem. A* **2008**, *112*, 1873−1879.
(49) Call, S. T.; Zubarev, D. Y.; Boldyrev, A. I. Global Minimum Structure Searches via Particle Swarm Optimization. *J. Comput. Chem.* **2007**, *28*, 1177−1186.
(50) Kirkpatrick, S.; Gelatt, C. D.; Vecchi, M. P. Optimization by Simulated Annealing. *Science* **1983**, *220*, 671−680.
(51) Perdew, J. P.; Burke, K.; Ernzerhof, M. Generalized Gradient Approximation Made Simple. *Phys. Rev. Lett.* **1996**, *77*, 3865−3868.
(52) Hay, P. J.; Wadt, W. R. Ab Initio Effective Core Potentials for Molecular Calculations - Potentials for the Transition-Metal Atoms Sc to Hg. *J. Chem. Phys.* **1985**, *82*, 270−283.
(53) Perdew, J. P.; Wang, Y. Accurate and Simple Analytic Representation of the Electron-Gas Correlation-Energy. *Phys. Rev. B* **1992**, *45*, 13244−13249.
(54) Figgen, D.; Rauhut, G.; Dolg, M.; Stoll, H. Energy-Consistent Pseudopotentials for Group 11 and 12 Atoms: Adjustment to Multi-Configuration Dirac-Hartree-Fock Data. *Chem. Phys.* **2005**, *311*, 227−244.
(55) Ross, R. B.; Powers, J. M.; Atashroo, T.; Ermler, W. C.; Lajohn, L. A.; Christiansen, P. A. Ab Initio Relativistic Effective Potentials with Spin-Orbit Operators IV. Cs through Rn. *J. Chem. Phys.* **1990**, *93*, 6654−6670.
(56) Dunning, T. H. Gaussian Basis Sets for Use in Correlated Molecular Calculations. I. The Atoms Boron through Neon and Hydrogen. *J. Chem. Phys.* **1989**, *90*, 1007−1023.
(57) Woon, D. E.; Dunning, T. H. Gaussian Basis Sets for Use in Correlated Molecular Calculations. III. The Atoms Aluminum through Argon. *J. Chem. Phys.* **1993**, *98*, 1358−1371.
(58) Casida, M. E.; Jamorski, C.; Casida, K. C.; Salahub, D. R. Molecular Excitation Energies to High-Lying Bound States from Time-Dependent Density-Functional Response Theory: Characterization and Correction of the Time-Dependent Local Density Approximation Ionization Threshold. *J. Chem. Phys.* **1998**, *108*, 4439−4449.
(59) Valiev, M.; Bylaska, E. J.; Govind, N.; Kowalski, K.; Straatsma, T. P.; Van Dam, H. J. J.; Wang, D.; Nieplocha, J.; Apra, E.; Windus, T. L.; et al. NWChem: A Comprehensive and Scalable Open-Source Solution for Large Scale Molecular Simulations. *Comput. Phys. Commun.* **2010**, *181*, 1477−1489.
(60) Zubarev, D. Y.; Boldyrev, A. I. Developing Paradigms of Chemical Bonding: Adaptive Natural Density Partitioning. *Phys. Chem. Chem. Phys.* **2008**, *10*, 5207−5217.
(61) Frisch, M. J. Trucks, G. W.; Schlegel, H. B.; Scuseria, G. E.; Robb, M. A.; Cheeseman, J. R.; Scalmani, G.; Barone, V.; Mennucci, B.; Petersson, G. A. et al. *Gaussian 09*; Gaussian: Wallingford, CT, 2009.
(62) Dennington, R.; Keith, T.; Millam, J. *GaussView*, Version 4.2.1; Semichem Inc.: Shawnee Mission, KS, 2006.
(63) Wolinski, K.; Hinton, J. F.; Pulay, P. Efficient Implementation of the Gauge-Independent Atomic Orbital Method for NMR Chemical-Shift Calculations. *J. Am. Chem. Soc.* **1990**, *112*, 8251−8260.
(64) Schleyer, P. V.; Maerker, C.; Dransfeld, A.; Jiao, H. J.; van Eikema Hommes, N. J. R. Nucleus-Independent Chemical Shifts: A Simple and Efficient Aromaticity Probe. *J. Am. Chem. Soc.* **1996**, *118*, 6317−6318.
(65) Martin, N. H.; Teague, M. R.; Mills, K. H. Computed NMR Shielding Effects over Fused Aromatic/Antiaromatic Hydrocarbons. *Symmetry* **2010**, *2*, 418−436.

(66) Wang, X. B.; Ding, C. F.; Wang, L. S. High Resolution Photoelectron Spectroscopy of C_{60}^-. *J. Chem. Phys.* **1999**, *110*, 8217−8220.
(67) Casey, S. M.; Leopold, D. G. Negative Ion Photoelectron Spectroscopy of Cr_2. *J. Phys. Chem.* **1993**, *97*, 816−830.
(68) Li, J.; Li, X.; Zhai, H. J.; Wang, L. S. Au_{20}: A Tetrahedral Cluster. *Science* **2003**, *299*, 864−867.
(69) Dekock, R. L.; Barbachyn, M. R. Electronic-Structure and Molecular Topology of Boron and Aluminum Suboxides. *J. Inorg. Nucl. Chem.* **1981**, *43*, 2645−2647.
(70) Archibong, E. F.; Sullivan, R. An Ab Initio Study of the Structures and Harmonic Vibrational Frequencies of M_2O_2 (M = Al, Ga, In, Tl). *J. Phys. Chem.* **1995**, *99*, 15830−15836.
(71) Lazzeretti, P. Assessment of Aromaticity via Molecular Response Properties. *Phys. Chem. Chem. Phys.* **2004**, *6*, 217−223.
(72) Aihara, J. I. Nucleus-Independent Chemical Shifts and Local Aromaticities in Large Polycyclic Aromatic Hydrocarbons. *Chem. Phys. Lett.* **2002**, *365*, 34−39.
(73) Greeff, C. W.; Lester, W. A., Jr.; Hammond, B. L. Elerctronic States of Al and Al_2 using Quantum Monte Carlo with and Effective Core Potential. *J. Chem. Phys.* **1996**, *104*, 1973.
(74) Pakiari, A. H.; Jamshidi, Z. Nature and Strength of M-S Bonds (M = Au, Ag, and Cu) in Binary Alloy Gold Clusters. *J. Phys. Chem. A* **2010**, *114*, 9212.
(75) Gingerich, K. A.; Blue, G. D. Mass Spectrometric Investigation of the Dissociation Energy of the Molecule AlAu and Estimated Bond Energies of Some Diatomic Intermetallic Compounds with Gold. *J. Chem. Phys.* **1973**, *59*, 185.